Measurement of Thermal Expansion Coefficient on Electric Cable Using X-Ray Digital Microradiography

Yessi Affriyenni
Department of Physics
State University of Malang
Malang, Indonesia
yessihasrizal@gmail.com

Gede Bayu Suparta
Department of Physics
Gadjah Mada University
Yogyakarta, Indonesia
gbsuparta@ugm.ac.id

Galandaru Swalaganata
Department of Mathematics Education
State Islamic Institute of Tulungagung
Tulungagung, Indonesia
galandaru.swalaganata@gmail.com

***Abstract*— Electric cable is a medium to conduct electrical energy. Expansion and contraction caused by thermal changes may result in an aging effect on the cable. This paper presents the way to observe the expansion in electrical cable due to thermal changes using the x-ray microradiography. The observed electric cables were NYA, NYAF, and NYM, each with cross-sectional areas of 1.5 mm^2 and 2.5 mm^2. The temperature was monitored using a DS18B20 sensor compiled into a microcontroller. In order to process and analyze the cables images, an *ImageJ* software was used. The image differences were compared based on the value of the digital image correlation. The physical analysis was carried out based on Adrian's FWHM and calculated using the regression method. The accurate structural dimension measurement using x-ray digital microradiography is about 50 μm/pixel. The average relative error measured was less than 3%.**

Keywords*— cable, thermal expansion, image correlation, digital microradiograph, x-ray

I. INTRODUCTION

Electric cable is a medium to conduct electrical energy. Basically, it consists of insulative and conductive parts. The electric cable is characterized by its current conducting capacity (ampacity). The ampacity is affected by the environmental factors such as temperature. The temperature of cable might be changed because of both the response of its resistivity to current changes and the changes in ambient temperature. Expansion caused by thermal changes may result in an aging effect on the cable. Furthermore, it may cause damage [1].

Cable quality is also influenced by its thermodynamics characteristic such as thermal expansion coefficient. The majority of instruments which had been developed to measure this characteristic are dilatometers, comparators, capacitance method, optical interferometry, and thermomechanical analysis but weaknesses are still found [2]. However, these conventional methods cannot detect the expansion of cable installed inside a building, as if it was installed inside the wall or between the ceiling and the roof without destroying the building itself. Thus, we're trying to find a method to detect the change of dimension occurred on the cable using a non-destructive method.

An x-ray micro-digital radiography system has been developed at the Department of Physics, Gadjah Mada University. It is a non-destructive testing method. It comprises a laboratory x-ray generator and an x-ray fluoroscopy image converter. The x-ray generator has a Molybdenum anode target. The x-ray fluoroscopy image converter as image detector comprises a fluorescence screen in dark cavity which is coupled with a CMOS digital camera to produce digital radiographs [3]. Based on the previous study, the accurate structural dimension measurement using this instrument is about 50 μm/pixel [4].

II. RESEARCH METHOD

The data was collected in Department of Physics, Gadjah Mada University Yogyakarta including metal cutting, metal drilling, metal welding, data acquisition, and data analysis. The research method followed the flowchart shown in Figure 1. Metal cutting, metal drilling, and metal welding for the heating set were done by following the design shown in Figure 2.

A customized x-ray digital micro-radiography system has been used for data acquisition as shown in Figure 3. The x-ray tube voltage and filament current were set at 40 keV and 30 mA consecutively. The transmitted x-ray from x-ray tube will be partially absorbed by the cable. The passed intensity will form analog radiography image in the fluorescence screens. The image was then captured and converted to be a digital image by CMOS camera. The images were saved in a hard disk of a computer. The images might be displayed and processed for further analysis.

The type of the electric cables for this study was NYA, NYAF, and NYM, which each has two cross-sectional area of 1.5 mm^2 and 2.5 mm^2. All cables were cut into 120 mm length. The conductor metal of these cables is known to be copper so the range of thermal expansion coefficient should be in the range of 16×10^{-6}/^{o}C to 18×10^{-6}/^{o}C [5]. Every cable was heated from 30^{o}C to 100^{o}C and then their images were collected for each 10^{o}C increment. The temperature changes were monitored by using DS18B20 waterproof temperature sensor compiled into the microcontroller. The measurement results were then displayed on the PC monitor by using the HyperTerminal software [6].

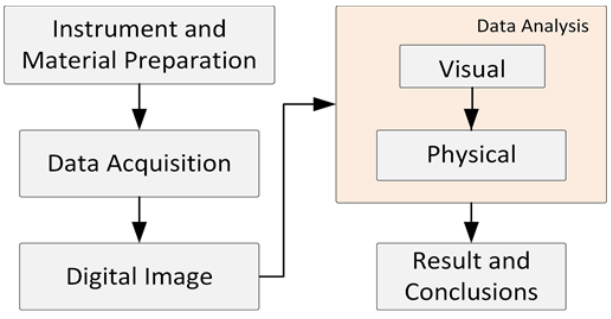

Fig. 1. Flowchart design.

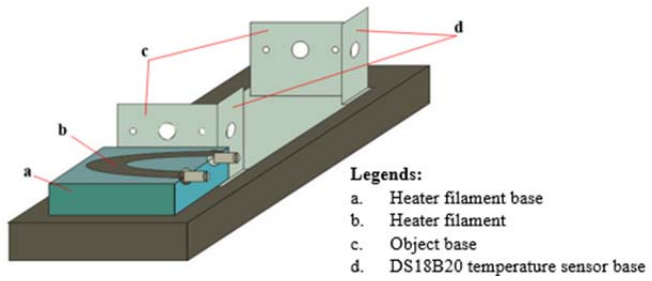

Fig. 2. Heater set design.

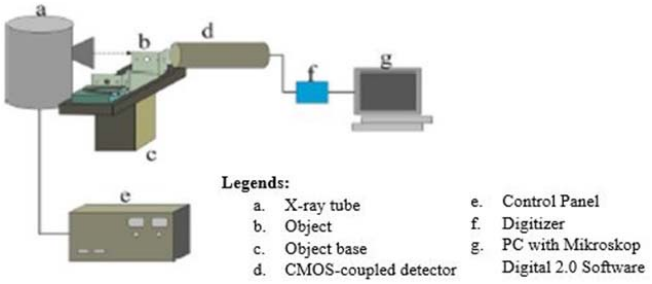

Fig. 3. The x-ray digital micro-radiography system.

In order to process and analyze the radiography images of the cables, an *ImageJ* software was used to analyze the acquired images [7]. Prior, the images were corrected to enhance the visibility and image sharpness.

This software was used for image processing and data analysis. In image processing stage, the images were corrected to remove background values and then added to itself to increase the sharpness [8]. Then, the images were cropped to show the edges only and the process of finding the edge was conducted [9].

Data analysis was conducted in two aspects including visual analysis and physical analysis. Visual analysis was conducted based on image elongation following temperature increment. The image differences were compared based on the value of the digital image correlation (DIC) which has been plugged into the *ImageJ* software [10]. The DIC value measurement follows Eq. 1 which is Pearson's Correlation Coefficient where f_i and g_i are the intensity of the i^{th} pixel in the 1st image and 2nd image respectively, f_{mean} and g_{mean} are the mean intensity of the 1st image and 2nd image consecutively [11].

The physical analysis was carried out based on Adrian's FWHM [12] to determine the initial and final pixel position of the edges due to temperature changes after the heating process. Position changes were analyzed based on the x-center value of Adrian's FWHM. Metals expansion coefficient was determined using least square fit method (regression method). The equation of thermal expansion is shown in Eq. 2 where L is the final length, L_0 is initial length, α is the coefficient of thermal expansion, and ΔT is temperature change [13].

$$C = \frac{\sum_{i=1}^{n}\left(f_i - \bar{f}\right)\left(g_i - \bar{g}\right)}{\sqrt{\sum_{i=1}^{n}\left(f_i - \bar{f}\right)^2 \sum_{i=1}^{n}\left(g_i - \bar{g}\right)^2}} \quad (1)$$

$$L = L_0 + \alpha \Delta T \quad (2)$$

III. Results and Analysis

In this study, scanning was done on each object and 5 images were obtained for each 10ºC increment. Every obtained image is representing the changes of position due to the changes of temperature. Figure 4a and 4b show the comparison of images before and after subtraction process. Image subtraction was done by subtracting the obtained image with a background image. Plot profiles which are shown in Figure 4c and 4d describe that the background value has been corrected proven by the curve at position range from 0 to 200 coincides with the x-axes in Figure 4d.

Figure 5 shows images and plot profile both before and after addition. The purpose of image addition in this study was to increase the contrast so the edges seemed clearer. Figure 5a and 5b show that there is brightness difference between both images and makes the edges seem clearer. Figure 5c and 5d are the plot profile for the images in Figure 5a and 5b that show no changes in object geometry just the change in gray value. Based on the corrected and normalized radiography images, the image has good contrast so that the edges can be shown clearly.

Table 1 shows image correlation coefficients of images in several temperatures relative to one another for NYA 1,5 object. The DIC value differences signify the geometrical changes occurred, and it is significant at 10ºC temperature change from 30ºC to 100ºC. Other image correlation coefficients for NYA 2.5, NYAF 1.5, NYAF 2.5, NYM 1.5, and NYM 2.5 are not shown because it show the similar trend to Table 1.

TABLE I. Image Correlation Coefficients for Heated NYA, NYAF, and NYM Cable

Type	Temperature (ºC)							
	30	40	50	60	70	80	90	100
NYA 1.5	1.000	1.000	1.000	1.000	0.999	1.000	1.000	1.000
NYA 2.5	1.000	1.000	1.000	1.000	1.000	0.999	0.999	0.999
NYAF 1.5	1.000	1.000	0.996	0.995	0.983	0.982	0.977	0.966
NYAF 2.5	1.000	0.999	0.990	0.977	0.975	0.975	0.974	0.973
NYM 1.5	1.000	0.997	0.996	0.994	0.985	0.983	0.960	0.947
NYM 2.5	1.000	1.000	0.999	0.998	0.998	0.998	0.998	0.982

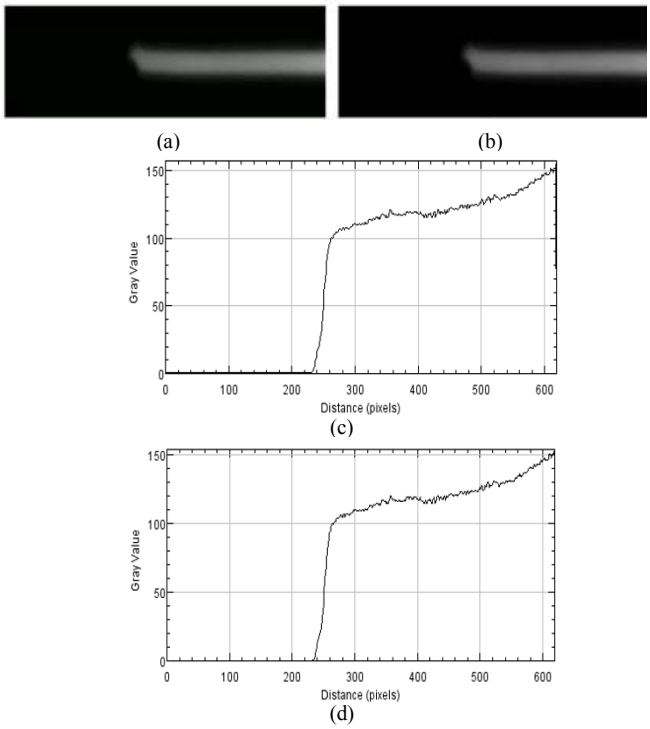

Fig. 4. Example of (a) Image before subtraction, (b) Image after subtraction, (c) Plot profile before subtraction having background gray value of 0, (d) Plot profile after subtraction having background gray value of 1.

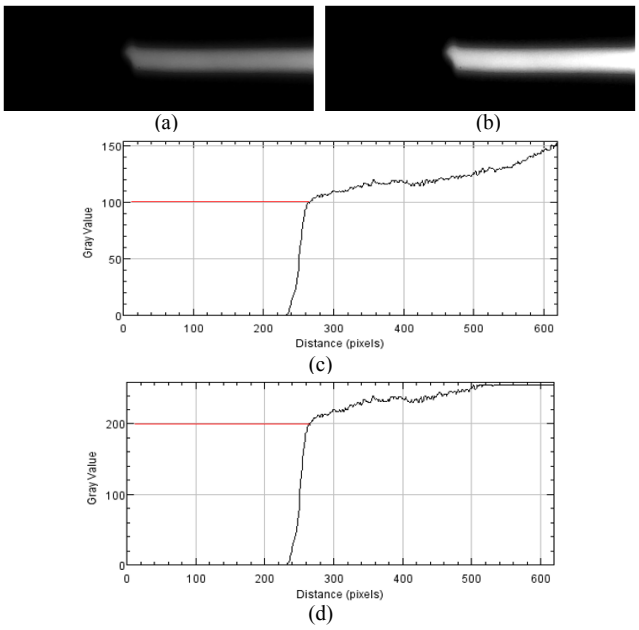

Fig. 5. Example of (a) Image before addition, (b) Image after addition, (c) Plot profile before addition, (d) Plot profile after addition.

Based on Table 1, the image of metal dilation was obtained for each object to show the changes in object geometry caused by its temperature change. Figure 6 shows metal dilation of NYA 1.5, NYA 2.5, NYAF 1.5, NYAF 2.5, NYM 1.5, and NYM 2.5.

The initial position of cable was measured at 30ºC temperature using Adrian's FWHM analysis gives the pixel position of the edge and its uncertainty in which it is related to the temperature change. The change of metal length can be observed based on the dilation of peak value on graph obtained for each temperature that's shown in Table 2 and Figure 7. Calibration procedure yielded on conversion from pixel to c.g.s. unit that is 220 $\pm$ 5 pixel equals to 1.5 cm.

Based on the obtained data listed in Table 2, the coefficient of thermal expansion was calculated by using least square fit method or regression method. This method was used because of its capability to determine the uncertainty for minimum length expansion. The linearity for data is shown in Figure 8. Based on the Pearson's *r* obtained from the graph, the data were confirmed to be linear so it could be analyzed using the least square method.

The calculated coefficients were then compared with a copper coefficient of thermal expansion range based on [5] that is 16×10^{-6}/ºC to 18×10^{-6}/ºC since the conductor are all made of copper and shown in Table 3.

Based on the results shown in Table 3, variances still exist in the experiment values but still in the range of the reference value. These might be caused by unknown prior treatment history of the cables in the factory before, whether it was wrought or cast. Furthermore, authors can't control how these cables were treated in the market, how it was rolled, to what degree had it being bent before. These unknown prior histories of specimen might influence the structures of copper. The differences might also be caused by specimen size, heating rate, or thermocouple position.

Based on the research process and the ability of the system to capture metal length changes, authors may state that X-Ray Digital Microradiography built in the department of physics at Gadjah Mada University in Yogyakarta-Indonesia is capable of observing thermal expansion phenomena.

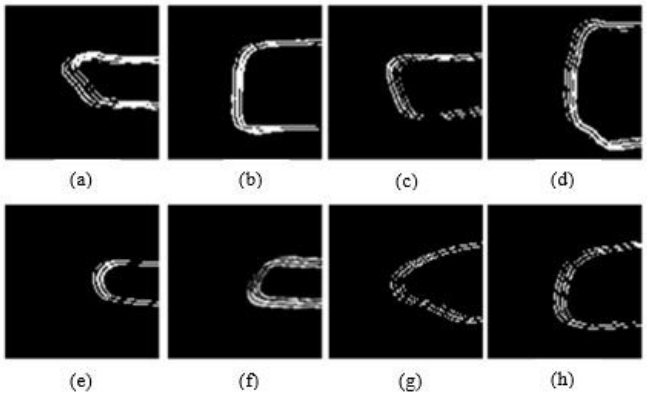

Fig. 6. Conductor dilation from 30ºC to 100ºC of (a) NYA 1.5, (b) NYA 2.5, (c) NYAF 1.5, (d) NYAF 2.5, (e) NYM 1.5 Blue, (f) NYM 1.5 Black, (g) NYM 2.5 Blue, (h) NYM 2.5 Black.

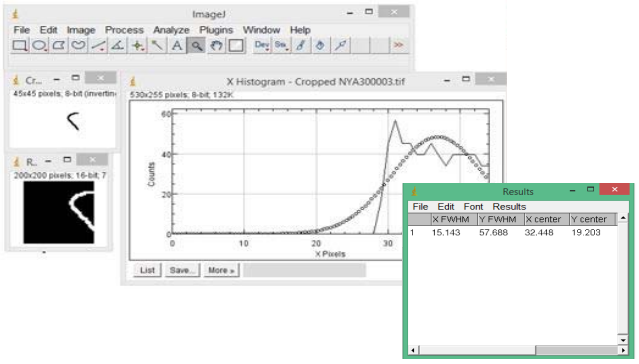

Fig. 7. The image analyzing process on NYA 1.5 at 30ºC temperature using Adrian's FWHM plugins.

TABLE II. METALS EDGE'S DILATION. (A) NYA 1.5, (B) NYA 2.5, (C) NYAF 1.5, (D) NYAF 2.5, (E) NYM 1.5 BLUE, (F) NYM 1.5 BLACK, (G) NYM 2.5 BLUE, (H) NYM 2.5 BLACK

$T(^oC)$	L_0 (cm)	dL (cm)
30	12.00±0.04	0
40	12.00±0.04	1.32×10^{-3}
50	12.00±0.04	3.71×10^{-3}
60	12.01±0.04	5.73×10^{-3}
70	12.01±0.04	8.03×10^{-3}
80	12.01±0.04	10.41×10^{-3}
90	12.01±0.05	11.80×10^{-3}
100	12.01±0.05	13.17×10^{-3}

(a)

$T(^oC)$	L_0 (cm)	dL (cm)
30	12.00 ± 0.02	0
40	12.00 ± 0.02	1.67×10^{-3}
50	12.00 ± 0.02	3.94×10^{-3}
60	12.01 ± 0.02	5.52×10^{-3}
70	12.01 ± 0.02	7.04×10^{-3}
80	12.01 ± 0.02	8.68×10^{-3}
90	12.01 ± 0.02	11.85×10^{-3}
100	12.02 ± 0.02	15.14×10^{-3}

(b)

$T(^oC)$	L_0 (cm)	dL (cm)
30	12.00 ± 0.05	0
40	12.00 ± 0.06	1.87×10^{-3}
50	12.00 ± 0.04	4.13×10^{-3}
60	12.01 ± 0.04	5.84×10^{-3}
70	12.01 ± 0.05	7.61×10^{-3}
80	12.01 ± 0.04	9.99×10^{-3}
90	12.01 ± 0.04	11.97×10^{-3}
100	12.01 ± 0.04	13.88×10^{-3}

(c)

$T(^oC)$	L_0 (cm)	dL (cm)
30	12.00±0.03	0
40	12.00±0.03	2.43×10^{-3}
50	12.00±0.03	4.16×10^{-3}
60	12.01±0.03	6.31×10^{-3}
70	12.01±0.03	8.55×10^{-3}
80	12.01±0.03	10.64×10^{-3}
90	12.01±0.03	12.25×10^{-3}
100	12.01±0.03	13.80×10^{-3}

(d)

$T(^oC)$	L_0 (cm)	dL (cm)
30	12.00±0.05	0
40	12.00±0.06	1.68×10^{-3}
50	12.00±0.08	3.78×10^{-3}
60	12.01±0.07	5.91×10^{-3}
70	12.01±0.08	7.64×10^{-3}
80	12.01±0.06	9.57×10^{-3}
90	12.01±0.07	12.06×10^{-3}
100	12.01±0.06	13.86×10^{-3}

(e)

$T(^oC)$	L_0 (cm)	dL (cm)
30	12.00±0.04	0
40	12.00±0.05	1.60×10^{-3}
50	12.00±0.05	3.27×10^{-3}
60	12.01±0.05	5.37×10^{-3}
70	12.01±0.05	7.51×10^{-3}
80	12.01±0.06	9.59×10^{-3}
90	12.01±0.06	11.28×10^{-3}
100	12.01±0.07	13.36×10^{-3}

(f)

$T(^oC)$	L_0 (cm)	dL (cm)
30	12.00±0.05	0
40	12.00±0.05	2.47×10^{-3}
50	12.00±0.05	4.67×10^{-3}
60	12.01±0.05	6.07×10^{-3}
70	12.01±0.05	8.08×10^{-3}
80	12.01±0.04	10.17×10^{-3}
90	12.01±0.05	12.38×10^{-3}
100	12.01±0.05	14.84×10^{-3}

(g)

$T(^oC)$	L_0 (cm)	dL (cm)
30	12.00±0.07	0
40	12.00±0.08	2.50×10^{-3}
50	12.00±0.06	4.39×10^{-3}
60	12.01±0.06	5.90×10^{-3}
70	12.01±0.07	7.45×10^{-3}
80	12.01±0.07	10.19×10^{-3}
90	12.01±0.07	12.87×10^{-3}
100	12.01±0.08	14.26×10^{-3}

(h)

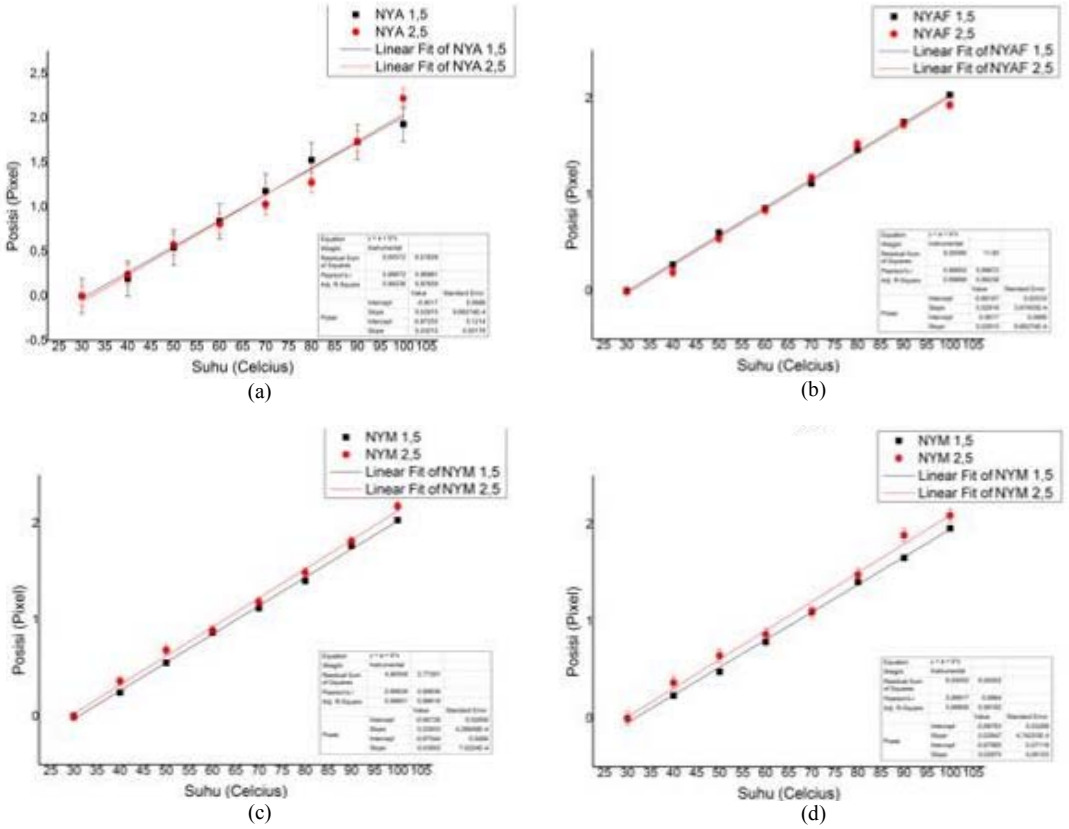

Fig. 8. Linearity graph of conductor dilation. (a) NYA, (b) NYAF, (c) NYM Blue, (d) NYM Black.

TABLE III. LINEARITY GRAPH OF CONDUCTOR DILATION. (A) NYA, (B) NYAF, (C) NYM 1.5 BLUE, (F) NYM 1.5 BLACK, (G) NYM 2.5 BLUE, (H) NYM 2.5 BLACK

Objects / Sizes		Linear Thermal Coefficient	
		1.5 mm² (×10⁻⁶/ºC)	**2.5 mm² (×10⁻⁶/ºC)**
NYA		16.6 ± 0.5	17 ± 1
NYAF		16.6 ± 0.2	16.6 ± 0.4
NYM	Blue	16.7 ± 0.2	17.1 ± 0.4
	Black	16.2 ± 0.3	16.9 ± 0.6

IV. CONCLUSION

The developed x-ray microradiography system has been attempted to use for observing metal expansion due to the heating process. From the experiment, the metal expansion can be examined based on the radiographs. Through careful measurement and analysis, it is possible to measure the coefficient of linear thermal expansion with an average relative error of less than 3%. Meanwhile, the measured linear thermal expansion varies in the range of reference values. Improvement may be achieved by better pretreatment, instrument improvements, and proper calibration.

ACKNOWLEDGMENT

The authors acknowledged the contribution of Lembaga Pengelola Dana Pendidikan (LPDP) under Ministry of Finance Indonesia for the financial support given to this work in 2016-2017.

REFERENCES

[1] G. F. Moore, *Electric Cables Handbook*. Liverpool: Blackwell Science, 1997.

[2] S. J. Bennett, "An absolute interferometric dilatometer," *J. Phys. E.*, vol. 10, no. 5, p. 525, 1977.

[3] G. B. Suparta, A. C. Louk, H. Kurniasari, and G. A. Wiguna, "The use of x-ray micro-digital radiography for clay material inspection," 2014, vol. 9234, p. 92340Y–9234–5.

[4] A. M. Y. Putranto, "Observation of Linear Thermal Expansion for Aluminium, Iron and Copper Using Digital X-Ray Micro-Radiograph," Gadjah Mada University, 2014.

[5] F. Cverna, *ASM Ready Reference: Thermal Properties of Metals*. Ohio: ASM International, 2002.

[6] C. Baumgartner *et al.*, *User's Manual HyperAccess for Windows*. Monroe: Hilgraeve Inc, 2000.

[7] T. Ferreira and W. Rasband, "ImageJ User Guide," 2012. [Online]. Available: https://imagej.nih.gov/ij/docs/guide/user-guide.pdf. [Accessed: 14-Apr-2018].

[8] G. Swalaganata, Muniri, and Y. Affriyenni, "Moving object tracking using hybrid method," in *2018 International Conference on Information and Communications Technology (ICOIACT)*, 2018, pp. 607–611.

[9] G. Swalaganata, D. R. Sulistyaningrum, and B. Setiyono, "Super-resolution imaging applied to moving object tracking," *J. Phys. Conf. Ser.*, vol. 893, no. 1, p. 12062, 2017.

[10] F. Hild and S. Roux, "Digital image correlation," in *Optical Methods for Solid Mechanics*, Weinheim: Wiley-VCH Verlag & Co., 2012, pp. 183–228.

[11] A. Miranda Neto, A. Victorino, I. Fantoni, D. Zampieri, J. Ferreira, and D. Lima, "Image Processing Using Pearson's Correlation Coefficient: Applications on Autonomous Robotics," in *2013 13th International Conference on Autonomous Robot Systems*, 2013, pp. 1–6.

[12] A. Martin, "Adrian's FWHM V1.1 code documentation," 2008. [Online]. Available: https://imagej.nih.gov/ij/plugins/fwhm/. [Accessed: 14-Apr-2018].

[13] J. R. Taylor, *An Introduction to Error Analysis: The Study of Uncertainties in Physical Measurements*. Sausalito: University Science Books, 1997.